Research Article

Advances in Mechanical Engineering

Advances in Mechanical Engineering
2020, Vol. 12(3) 1–18

DOI: 10.1177/1687814020913667
journals.sagepub.com/home/ade
SAGE

Minimum-jerk trajectory planning pertaining to a translational 3-degree-of-freedom parallel manipulator through piecewise quintic polynomials interpolation

Song Lu[1], Bingxiao Ding[2] and Yangmin Li[3]

Abstract

This article aims to present a minimum-jerk trajectory planning approach to address the smooth trajectory generation problem of 3-prismatic-universal-universal translational parallel kinematic manipulator. First, comprehensive kinematics and dynamics characteristics of this 3-prismatic-universal-universal parallel kinematic manipulator are analyzed by virtue of the accepted link Jacobian matrices and proverbial virtual work principle. To satisfy indispensable continuity and smoothness requirements, the discretized piecewise quintic polynomials are employed to interpolate the sequence of joints' angular position knots which are transformed from these predefined via-points in Cartesian space. Furthermore, the trajectory planning problem is directly converted into a constrained nonlinear multi-variables optimization problem of which objective function is to minimize the maximum of the joints' angular jerk throughout the whole trajectory. Finally, two typical application simulations using the reliable sequential quadratic programming algorithm demonstrate that this proposed minimum-jerk trajectory planning approach is of explicit feasibility and appreciable effectiveness.

Keywords

Trajectory planning, parallel kinematic manipulator, jerk, the principle of virtual work, piecewise quintic polynomials

Date received: 6 November 2019; accepted: 19 February 2020

Handling Editor: Jose Herreros

Introduction

The last three decades have witnessed a considerable development of parallel kinematic manipulators (PKMs) which can be treated as positive encouraging candidates for many advanced automation processes and digitalization applications.[1–5] Undoubtedly, the apparent advantages of PKMs are low moving inertia, high stiffness, high dexterity, and high payload-to-weight ratio. These distinct characteristics determine PKMs' increasing widespread utilization in the fields of industrial assembly and practical operations such as high-speed picking and placing,[6] vibration simulator,[7] precise microsurgery,[8] cardiopulmonary resuscitation[9] and so on. When implementing a specific practical engineering task (assembly, spot welding, palletization, or three-dimensional printing), for the sake of decreasing vibration deformation and improving positioning accuracy in the movement, the realistic trajectory

[1]Department of Electromechanical Engineering, Faculty of Science and Technology, University of Macau, Macao, China
[2]School of Physics and Electromechanical Engineering, Jishou University, Jishou, China
[3]Department of Industrial and Systems Engineering, The Hong Kong Polytechnic University, Kowloon, Hong Kong

Corresponding author:
Bingxiao Ding, School of Physics and Electromechanical Engineering, Jishou University, Jishou 416000, China.
Email: bingxding@hotmail.com

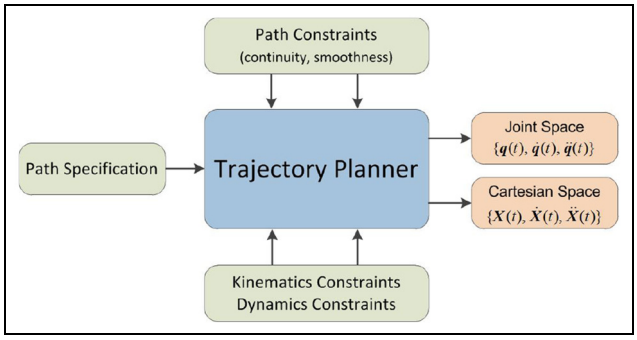

Figure 1. Brief framework of general trajectory planning.

should possess remarkable continuity, eminent smoothness, and high operation efficiency.[10]

The trajectory planning issue that establishes a parametric function concerning time under several different unambiguous constraints is attracting prodigious research interest between academia and industry.[11–13] As a particularly critical part of PKMs design and system scheme, the accurate definition of trajectory can directly affect the choice of drive motors and reduction gears, vibrations, and efforts impacted on the mechanical structure, and tracking accuracy throughout the planned motion. In other words, the actual trajectory determines its real-time kinematics and dynamics performance of PKMs.[14,15] If the trajectory has a continuous curvature or even has a continuous higher order derivative of curvature, it is believed to be smooth.[16] The brief framework of common trajectory planning is illustrated in Figure 1, trajectory planner formulates a specific excellent trajectory that must satisfy the indispensable path constraints, kinematics constraints, and dynamic constraints. In the existing scientific and technological literature of robots and manipulators, there are many concrete considerations regarding to traditional trajectory planning topic, the most common of which are minimum execution time,[17–19] minimum energy[20–22] (or actuator effort), and minimum jerk (i.e. the third-order derivative of position curve with time).[23–26] The presence of discontinuity and roughness on the trajectory has been found to correlate with a drastically increase of large jerk value reported in the past several decades.[27,28] Limiting the system maximum jerk value, which can diminish vibration influence motivated by the dominant vibration factor of the axis, reduce structure wear and resonance frequency emergence, improve tracking precision, and enhance trajectory smoothness and operational stability, is highly recommended to cope with the trajectory planning problem.[29–31] Minimum-jerk trajectory planning theory and methodology relating to traditional serial kinematic manipulators have been intensively discussed and investigated by numerous researchers. Piazzi and Visioli[23] developed a concise approach to globally minimize the maximum of the absolute value of jerk along a trajectory which was easily expressed through cubic splines. The execution time was set a priori, and it was worth noting that the effect of dynamics property was without taking into account. Macfarlane and Croft[24] put forward a jerk-limited and near-time-optimal trajectory planning strategy applied on a general 6-degree-of-freedom (DOF) manipulator, where the accompanying point-to-point trajectory was interpolated using the piecewise fifth-order polynomial function. Gasparetto and colleagues[15,26] introduced a minimum time-jerk trajectory planning algorithm of which objective function was to reach a reasonable compromise between the overall task execution time and the total integral value of squared jerk. For the sake of formulation of minimum-jerk trajectory planning for surface-mount assembly robots, Gyorfi and Wu[25] utilized the discretized quintic polynomial curve to obtain an expected trajectory with appealing smoothness and jerk-limited property. To cope with a notable constrained velocity-level path planning issue for traditional mobile robots, Guarino Lo Bianco[32] introduced a seven-segment parabolic velocity curve to fulfill the complicated minimum-jerk trajectory planning assignment of which objective was to minimize the maximum of longitudinal jerk. To bring out a minimum-time trajectory for a two-DOF translational PKM in Cartesian space, Huang et al.[33] optimized the whole travel time as well as imposing the path jerk limitation as an indispensable constraint condition in order to achieve satisfactory smooth performance. For an unordinary high-speed 2-DOF two-dimensional PKM different from Huang et al.,[33] Hu et al.[34] proposed an optimal time trajectory planning method using piecewise cubic polynomials in joint space while the inherent dynamic constraints were not taken into full consideration. In general, jerk-level trajectory planning approaches can be frequently employed for addressing the senior complicated trajectory planning problems of traditional manipulators with satisfying stringent continuity requirements and sufficient smooth conditions. Unfortunately, to the best of our knowledge, little research has been devoted to jerk-based trajectory planning techniques applied to three-dimensional PKMs scenarios. It is the increasing demand for formulation of smooth trajectory of PKMs that facilitates the profound theoretical research, imperative practical application, and extensive engineering development of the jerk-based trajectory planning concept.

Generally, cubic polynomials are often used in smooth trajectory generation;[35] however, they provide a constant jerk profile, and they are not applicable to high-level trajectory planning. Higher order polynomials are needed to generate smoother jerk profile. The lowest order polynomials to guarantee the smoothness of jerk profile at the sequence of via-points are quintic

polynomials of which jerk profile are quadratic polynomials and with C^2 continuity.[23] Also, complete dynamics model analysis without neglecting the inertial and gravitational properties of the struts is essential for trajectory planning. The joints' actuating torques specific for the given trajectory should not exceed the maximum output torque of driving motors. Due to significant complexity and strong non-linearity in PKMs dynamic equations, the principle of virtual work has high priority over the dynamics analysis approaches of parallel manipulators. Since the generalized trajectory planning problem is typically a complex constrained programming problem with high dimension, non-linearity and non-convexity properties, as well as considering the control system exerts directly on active joints rather than end effector, a dedicated kinematics inversion process is required to equivalently transform the prerequisite path expressed in Cartesian space into a specific corresponding joints' profile and thereby trajectory planning is usually carried out in joint space. In addition, it is important to note that trajectory planning in joint space can prevent the tricky troubles resulting from kinematic singularities and manipulator redundancy.[14]

The practical implication of jerk-based trajectory planning is that since the jerk peak values are limited rationally during the thorough motion period, the optimized smooth trajectory would significantly contribute to reducing structure wear, suppressing dominating vibration, improving tracking accuracy, and potentially extend life cycle. To develop a desirable smooth trajectory for PKMs, this article presents a minimum-jerk trajectory planning approach applied to a 3-prismatic-universal-universal (3-PUU, the underline represents active joint) translational PKM. The remainder of this article is organized as follows. We perform essential kinematics analysis of the 3-PUU PKM in the second section, including position analysis, velocity analysis and acceleration analysis. In the third section, the formulation of complete inverse dynamics model relies on the virtual work principle, where the inertial property and gravitational quality of the struts are not ignored. The forth section describes the detailed process of generating the minimum-jerk trajectory that minimizes the maximum value of the absolute jerk value using piecewise quintic polynomials. Simulation results to demonstrate the effectiveness and feasibility of this proposed minimum-jerk trajectory planning strategy are provided in the fifth section. Finally, concluding remarks are shown in the last section.

Kinematics analysis

As shown in Figure 2, the generalized vertical-distributed 3-PUU PKM is employed a closed-loop

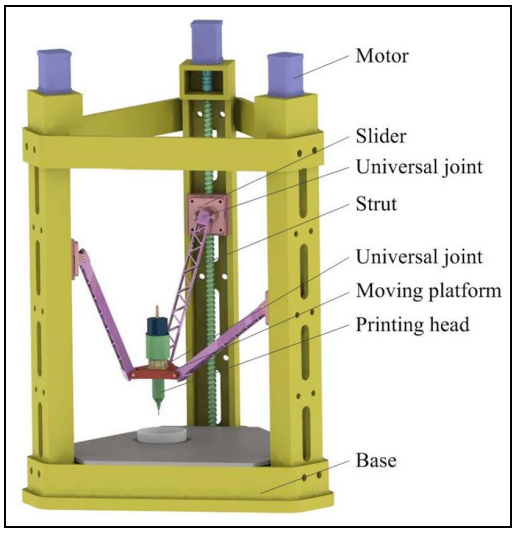

Figure 2. 3D model of the vertical-distributed 3-PUU parallel manipulator.

geometric characteristic structure which clearly consists of a stationary base, a movable platform, and three kinematic chains with uniform configuration. For every definite kinematic chain, universal joints are utilized to seamlessly connect the slider and strut, followed by association between the strut and moving platform. To generate translational motion of prismatic joint directly, the slider and guideway of a linear leadscrew assembly subsystem are matched and fitted to each other. Note that the three straight guideways are equipped into ideal central axisymmetric layout and perpendicular to stationary base, which allows the overall structure to withstand deformation caused by inertial loads. It is worthy pointing out that the moving platform's three specific translational DOFs in X, Y, and Z direction necessitate the satisfaction of the definitive geometric conditions, that is, in each PUU kinematic chain, the axis of the first revolute joint of upper U joint needs to be parallel to that of the first revolute joint of lower U joint, and the axis of the second revolute joint of upper U joint needs to be parallel to that of the second revolute joint of lower U joint. Without loss of generality, as indicated in Figure 3, the reference frame $O-xyz$ is located with O at the center of the equilateral triangle $\Delta B_1B_2B_3$ attached to stationary base. Similarly, the moving frame $O'-x'y'z'$ is located with O' at the center of the equilateral triangle $\Delta A_1A_2A_3$ attached to moving platform. The x-axis is regulated to orientate $\overrightarrow{OB_1}$, and z-axis is normal to $\Delta B_1B_2B_3$. Since moving platform is provided with three independent translational DOFs, $\boldsymbol{r} = [x, y, z]^T$ is used to define the position vector relative to the reference coordinate system $O-xyz$. Furthermore, observing from the topview as shown in Figure 4, the moving platform is restricted in a cylinder geometry with radius R.

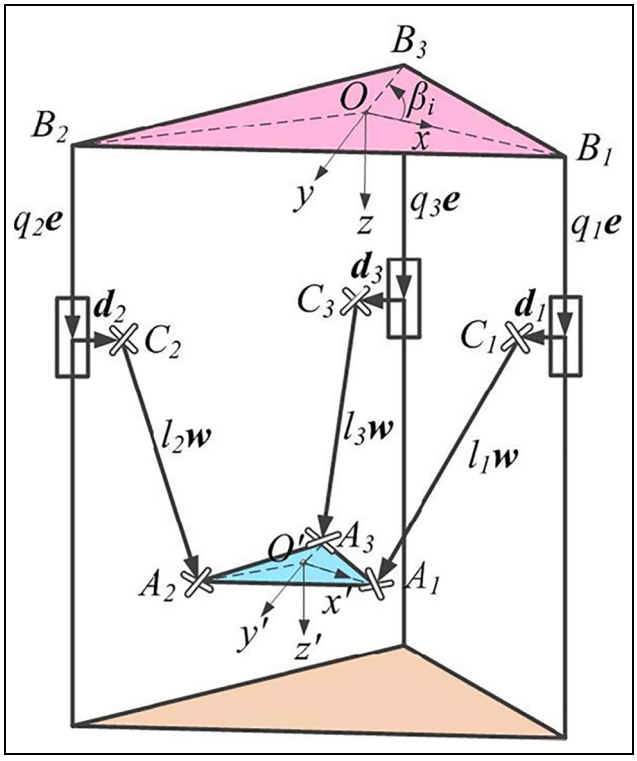

Figure 3. Simplified sketch of the 3-PUU PKM.

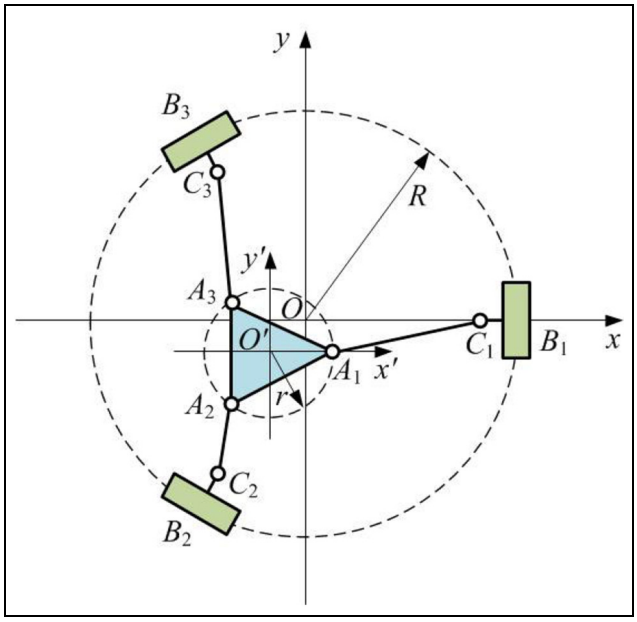

Figure 4. Topview of the vertical-arranged 3-PUU PKM.

Inverse position analysis

Give the position of moving platform, a primary closed-loop vector equation is intuitively established to determine the displacement of active joints

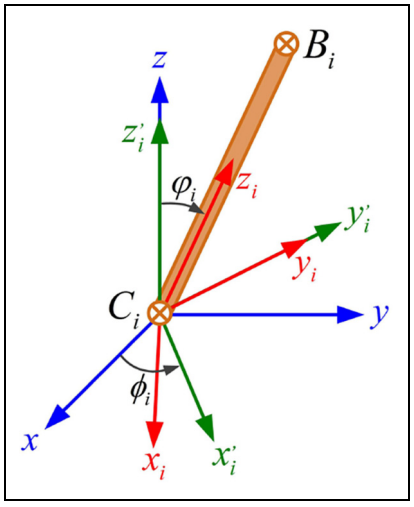

Figure 5. Conversion illustration of the local coordinate system.

$$\boldsymbol{r} = \boldsymbol{b}_i + q_i\boldsymbol{e} + \boldsymbol{d}_i + l\boldsymbol{w}_i - \boldsymbol{a}_i, (i = 1, 2, 3) \tag{1}$$

where $\boldsymbol{a}_i = [s\cos\beta_i, -s\sin\beta_i, 0]^T$, $\boldsymbol{b}_i = [S\cos\beta_i, -S\sin\beta_i, 0]^T$, $\boldsymbol{d}_i = [-d\cos\beta_i, d\sin\beta_i, 0]^T$, $\boldsymbol{e} = [0, 0, 1]^T \cdot s$, S, q_i, β_i, and l denote the radius of moving platform, the radius of fixed base, the linear displacement of slider i, the angle of point B_i in the coordinate $O - xyz$, and the length of the strut, respectively. $\boldsymbol{e}$, $\boldsymbol{w}_i$, $\boldsymbol{d}_i$, $\boldsymbol{a}_i$, and $\boldsymbol{b}_i$ represent the unit vector along leadscrew, the unit vector along strut, the vector from leadscrew to center point of universal joint C_i, the position vector of point A_i in the coordinate $O' - x'y'z'$, and the position vector of point B_i in the coordinate $O - xyz$, respectively.

As depicted in Figure 5, two independent Euler angles ϕ_i and φ_i are adopted to accurately explicate the concrete orientation of each strut with respect to the reference coordinate system, which can be readily visualized a rotation of ϕ_i about the z_i-axis resulting in a (x_i', y_i', z_i') system followed by another rotation of φ_i about the rotated y_i'−axis. Consequently, the rotation matrix of strut i can be obtained

$$^o\boldsymbol{R}_i = \begin{bmatrix} c\phi_i c\varphi_i & -s\phi_i & c\phi_i s\varphi_i \\ s\phi_i c\varphi_i & c\phi_i & s\phi_i s\varphi_i \\ -s\varphi_i & 0 & c\varphi_i \end{bmatrix} \tag{2}$$

where s and c represent *sin* and *cos*, respectively.

Equating the third column of $^o\boldsymbol{R}_i$ to $\boldsymbol{w}_i$ yields

$$\boldsymbol{w}_i = [c\phi_i s\varphi_i \quad s\phi_i s\varphi_i \quad c\varphi_i]^T \tag{3}$$

Solving equation (3) for ϕ_i and φ_i leads to

$$\begin{cases} c\varphi_i = w_{iz}, s\varphi_i = \sqrt{w_{ix}^2 + w_{iy}^2}, & (0 \leqslant \varphi \leqslant \pi) \\ s\phi_i = w_{iy}/s\varphi_i, c\phi_i = w_{ix}/s\varphi_i \end{cases} \tag{4}$$

Taking the Euclidean norm of equation (1) yields

$$q_i = \boldsymbol{r}^T\boldsymbol{e} - \sqrt{(\boldsymbol{r}^T\boldsymbol{e})^2 - \|\boldsymbol{r} + \boldsymbol{a}_i - \boldsymbol{b}_i - \boldsymbol{d}_i\|^2 + l^2} \quad (5)$$

and

$$\boldsymbol{w}_i = \frac{\boldsymbol{r} + \boldsymbol{a}_i - \boldsymbol{b}_i - \boldsymbol{d}_i - q_i\boldsymbol{e}}{l} \quad (6)$$

Forward position analysis

As a necessary and crucial step in trajectory planning procedure for parallel manipulator, the forward position analysis involves determining the position vector $\boldsymbol{r}$ of moving platform on the premise of a given set of inputs q_i. For convenience, equation (1) can be further rearranged and rewritten as

$$\boldsymbol{r} - (\boldsymbol{b}_i + \boldsymbol{d}_i - \boldsymbol{a}_i) - q_i\boldsymbol{e} = \boldsymbol{r} - \boldsymbol{r}_{0i} - q_i\boldsymbol{e} = l\boldsymbol{w}_i \quad (7)$$

where

$$\begin{aligned}\boldsymbol{r}_{0i} &= [(S-d-s)\cos\beta_i, (-S+d+s)\sin\beta_i, 0]^T \\ &= [x_{0i}, y_{0i}, z_{0i}]^T\end{aligned} \quad (8)$$

Taking Euclidean norm on both sides of equation (7) gives

$$q_1^2 - 2q_1z + (x-x_{01})^2 + (y-y_{01})^2 + z^2 - l^2 = 0 \quad (9)$$

$$q_2^2 - 2q_2z + (x-x_{02})^2 + (y-y_{02})^2 + z^2 - l^2 = 0 \quad (10)$$

$$q_3^2 - 2q_3z + (x-x_{03})^2 + (y-y_{03})^2 + z^2 - l^2 = 0 \quad (11)$$

Subtracting equation (9) from equation (10), we obtain

$$\begin{aligned}&(q_2^2 - q_1^2) - 2(q_2 - q_1)z + (x_{02}^2 - x_{01}^2) - 2(x_{02} - x_{01})x \\ &+ (y_{02}^2 - y_{01}^2) - 2(y_{02} - y_{01})y = 0\end{aligned} \quad (12)$$

Subtracting equation (11) from equation (10), we obtain

$$\begin{aligned}&(q_2^2 - q_3^2) - 2(q_2 - q_3)z + (x_{02}^2 - x_{03}^2) - 2(x_{02} - x_{03})x \\ &+ (y_{02}^2 - y_{03}^2) - 2(y_{02} - y_{03})y = 0\end{aligned} \quad (13)$$

Substituting equation (8) into equation (12) leads to

$$(q_2^2 - q_1^2) - 2(q_2 - q_1)z + (3x - \sqrt{3}y)(S-d-s) = 0 \quad (14)$$

Substituting equation (8) into equation (13) leads to

$$(q_2^2 - q_3^2) - 2(q_2 - q_3)z - 2\sqrt{3}y(S-d-s) = 0 \quad (15)$$

Combining equation (14) with equation (15), and solving the primary three-variable algebraic equations, we can easily obtain

$$x = \frac{\left(q_1^2 - \frac{1}{2}q_2^2 - \frac{1}{2}q_3^2\right) - (2q_1 - q_2 - q_3)z}{3(S-d-s)} \quad (16)$$

$$y = \frac{(q_2^2 - q_3^2) - 2(q_2 - q_3)z}{2\sqrt{3}(S-d-s)} \quad (17)$$

By incorporating equations (16) and (17) into equation (10), we acquire a general quadratic equation with respect to the variable z, namely

$$G_1z^2 + G_2z + G_3 = 0 \quad (18)$$

where

$$\begin{cases} G_1 = \dfrac{(2q_1 - q_2 - q_3)^2 + 3(q_2 - q_3)^2}{9(S-d-s)^2} + 1 \\ G_2 = \dfrac{-(2q_1^2 - q_2^2 - q_3^2)(2q_1 - q_2 - q_3) - 3(q_2^2 - q_3^2)(q_2 - q_3)}{9(S-d-s)^2} \\ \quad -\dfrac{2}{3}(q_1 + q_2 + q_3) \\ G_3 = \dfrac{(2q_1^2 - q_2^2 - q_3^2)^2 + 3(q_2^2 - q_3^2)^2}{36(S-d-s)^2} + (S-d-s)^2 \\ \quad + \dfrac{1}{3}(q_1^2 + q_2^2 + q_3^2) - l^2 \end{cases} \quad (19)$$

According to the structural characteristics and practical situation of this 3-PUU physical architecture, the position of moving platform in z direction can be deduced as

$$z = \frac{-G_2 + \sqrt{G_2^2 - 4G_1G_3}}{2G_1} \quad (20)$$

Substituting equation (20) into equations (16) and (17), the value of x and y are derived directly. One potential advantage is that thanks to its pronounced configuration and distinctive geometric layout, there will always exist a unique solution in the forward position analysis with respect to this vertical-distributed 3-PUU PKM, which indicates that the dimensional structure of this 3-PUU mechanical PKM can be invariably confirmed and determined under the precondition of the known input joint value.

Inverse velocity analysis

Taking the derivative of equation (1) with respect to time, the velocity equations of moving platform are described as

$$\boldsymbol{v} = \dot{q}_i\boldsymbol{e} + l\boldsymbol{\omega}_i \times \boldsymbol{w}_i, (i = 1, 2, 3) \quad (21)$$

where $\boldsymbol{v}$, $\dot{q}_i$, and $\boldsymbol{\omega}_i$ stand for the velocity of moving platform, velocity of ith slider, and angular velocity of ith strut, respectively.

Utilizing dot multiplication on both sides of equation (21) with vector $\boldsymbol{w}_i$ leads to the critical mapping relationship between the velocity of slider and the velocity of moving platform, resulting in

$$\dot{q}_i = \frac{\boldsymbol{w}_i^T}{\boldsymbol{w}_i^T \boldsymbol{e}} \boldsymbol{v} \tag{22}$$

Then, equation (22) needs to be rearranged briefly and written in a succinct matrix form

$$\dot{\boldsymbol{q}} = \boldsymbol{J}_q^{-1} \boldsymbol{J}_x \dot{\boldsymbol{X}} = \boldsymbol{J} \dot{\boldsymbol{X}} \tag{23}$$

$$\boldsymbol{J} = [\boldsymbol{J}_1, \boldsymbol{J}_2, \boldsymbol{J}_3]^T = \left[\frac{\boldsymbol{w}_1^T}{\boldsymbol{w}_1^T \boldsymbol{e}}, \frac{\boldsymbol{w}_2^T}{\boldsymbol{w}_2^T \boldsymbol{e}}, \frac{\boldsymbol{w}_3^T}{\boldsymbol{w}_3^T \boldsymbol{e}} \right]^T \tag{24}$$

where $\dot{\boldsymbol{q}} = [\dot{q}_1, \dot{q}_2, \dot{q}_3]^T$ denote the vector that incorporates the velocity of sliders, and $\dot{\boldsymbol{X}} = [\dot{x}, \dot{y}, \dot{z}]^T$ represents the velocity vector of moving platform. $\boldsymbol{J}$ is the renowned Jacobian matrix with three rows and three columns.

Link linear velocity and angular velocity analysis

It is important to point out that strut i cannot spin around its own longitudinal aixs; thus, $\boldsymbol{w}_i^T \boldsymbol{\omega}_i = 0$. Furthermore, executing cross-multiplication on both sides of equation (21) with the vector $\boldsymbol{w}_i$, the angular velocity of the ith strut in the fixed frame $O - xyz$ can be achieved

$$\boldsymbol{\omega}_i = \frac{1}{l} \tilde{\boldsymbol{w}}_i (\boldsymbol{E}_3 - \boldsymbol{e}\boldsymbol{J}_i) \boldsymbol{v} = \boldsymbol{J}_{\omega i} \boldsymbol{v} \tag{25}$$

where $\boldsymbol{E}_3$ represents the 3×3 identity matrix and $\tilde{\boldsymbol{w}}_i$ represents the skew-symmetric matrix of $\boldsymbol{w}_i$; notably

$$\tilde{\boldsymbol{w}}_i = \begin{bmatrix} 0 & -w_{iz} & w_{iy} \\ w_{iz} & 0 & -w_{ix} \\ -w_{iy} & w_{ix} & 0 \end{bmatrix} \tag{26}$$

The velocity of the center of the ith strut expressed in the reference frame $O - xyz$ is

$$\boldsymbol{v}_i = \dot{q}_i \boldsymbol{e} + \boldsymbol{\omega}_i \times \left(\frac{l \boldsymbol{w}_i}{2} \right) \tag{27}$$

Substituting equation (25) into equation (27), then taking a rational simplification yields

$$\boldsymbol{v}_i = \left(\boldsymbol{e}\boldsymbol{J}_i - \frac{1}{2} \tilde{\boldsymbol{w}}_i^2 (\boldsymbol{E}_3 - \boldsymbol{e}\boldsymbol{J}_i) \right) \boldsymbol{v} = \boldsymbol{J}_{vi} \boldsymbol{v} \tag{28}$$

The linear velocity and angular velocity of strut i can be further rearranged into a general matrix form, that is

$$\begin{bmatrix} \boldsymbol{v}_i \\ \boldsymbol{\omega}_i \end{bmatrix} = \begin{bmatrix} \boldsymbol{J}_{vi} \\ \boldsymbol{J}_{\omega i} \end{bmatrix} \boldsymbol{v} = \boldsymbol{J}_{v\omega i} \boldsymbol{v} \tag{29}$$

where $\boldsymbol{J}_{v\omega i}$ is stated the link Jacobian matrices (LJMs).[36] Unlike the preliminary concept defined in Tsai,[36] however, the LJMs presented in this article refer to the straightforward mapping relation between the velocity of platform and the velocity of the struts, which is particularly expressed in the reference frame instead of the local coordinates.

Inverse acceleration analysis

Similarly, taking the necessary derivative of equation (21) with respect to time, we can achieve

$$\boldsymbol{a} = \ddot{q}_i \boldsymbol{e} + l[\dot{\boldsymbol{\omega}}_i \times \boldsymbol{w}_i + \boldsymbol{\omega}_i \times (\boldsymbol{\omega}_i \times \boldsymbol{w}_i)] \tag{30}$$

where $\boldsymbol{a}$, $\ddot{q}_i$, and $\dot{\boldsymbol{\omega}}_i$ denote the acceleration of moving platform, acceleration of the ith slider, and angular acceleration of the ith strut, respectively.

The next step is to perform dot multiplication on both sides of equation (30) by $\boldsymbol{w}_i$, which results in

$$\ddot{q}_i = \frac{\boldsymbol{w}_i^T}{\boldsymbol{w}_i^T \boldsymbol{e}} \boldsymbol{a} + \frac{l}{\boldsymbol{w}_i^T \boldsymbol{e}} \tag{31}$$

Furthermore, equation (31) can be represented as

$$\ddot{\boldsymbol{q}} = \boldsymbol{J} \ddot{\boldsymbol{X}} + \boldsymbol{U} \tag{32}$$

$$\boldsymbol{U} = \left[\frac{l}{\boldsymbol{w}_1^T \boldsymbol{e}}, \frac{l}{\boldsymbol{w}_2^T \boldsymbol{e}}, \frac{l}{\boldsymbol{w}_3^T \boldsymbol{e}} \right]^T \tag{33}$$

where $\ddot{\boldsymbol{q}} = [\ddot{q}_1, \ddot{q}_2, \ddot{q}_3]^T$ denote the vector that incorporates the acceleration of sliders and $\ddot{\boldsymbol{X}} = [\ddot{x}, \ddot{y}, \ddot{z}]^T$ represents the acceleration vector of moving platform. Clearly, the nonlinear transition relationship from end-effector's acceleration in operational space to driving joints' acceleration is achieved.

Link linear acceleration and angular acceleration analysis

Performing cross-multiplication on both sides of equation (30) with the vector $\boldsymbol{w}_i$, the angular acceleration of strut the i can be obtained as

$$\dot{\boldsymbol{\omega}}_i = \frac{1}{l} \tilde{\boldsymbol{w}}_i (\boldsymbol{a} - \ddot{q}_i \boldsymbol{e}) = \boldsymbol{J}_{\omega i} \boldsymbol{a} - \frac{\tilde{\boldsymbol{w}}_i \boldsymbol{e}}{\boldsymbol{w}_i^T \boldsymbol{e}} \tag{34}$$

Taking the time derivative of equation (27), it leads to

$$\begin{aligned} \dot{\boldsymbol{v}}_i &= \ddot{q}_i \boldsymbol{e} + \dot{\boldsymbol{\omega}}_i \times \left(\frac{l \boldsymbol{w}_i}{2} \right) + \boldsymbol{\omega}_i \times \left(\frac{l}{2} \boldsymbol{\omega}_i \times \boldsymbol{w}_i \right) \\ &= \ddot{q}_i \boldsymbol{e} - \frac{l \boldsymbol{w}_i}{2} - \frac{l}{2} \tilde{\boldsymbol{w}}_i \dot{\boldsymbol{\omega}}_i \end{aligned} \tag{35}$$

Substituting equations (31) and (34) into equation (35), and taking a justified simplification lead to the linear acceleration of strut i, that is

$$\dot{\boldsymbol{v}}_i = \boldsymbol{J}_{vi}\boldsymbol{a} + \frac{l}{2}\left(\frac{\tilde{\boldsymbol{w}}_i^2\boldsymbol{e}}{\boldsymbol{w}_i^T\boldsymbol{e}} + \frac{2\boldsymbol{e}}{\boldsymbol{w}_i^T\boldsymbol{e}} - \boldsymbol{w}_i\right) \tag{36}$$

Eventually, complete inverse kinematics modeling is carried out where the link linear acceleration and link angular acceleration play an indispensable role in establishing, analyzing, and estimating the thorough dynamics model.

Dynamics modeling

Except the exhaustive kinematics equations analyzed above, the investigation of dynamics features is essential to the smooth trajectory planning of 3-PUU PKM.[37] First and foremost, we propose two prevalent hypotheses: (1) even though tiny elastic deformations of lightweight struts are inevitable in practice process, all components existing in the whole mechanical system are deemed ideal rigid bodies, which means that they can withstand the applied forces and do not deform; (2) the effect of frictional force among the joints and active components is negligible, and there is no energy loss caused by friction, consequently, the exclusive variation of virtual work is affected directly by the movement of the input and output forces/torques. Based on the system complexity and calculation efficiency, we apply the acquainted virtual work principle to conduct the subsequent dynamics analysis.

Dynamics analysis of the substructure system

From systemic energy perspective, the entire system can be reasonably split into four substructure aspects based on energy coupling principle, including

1. *Applied forces of the moving platform*. In general, the applied forces and inertia forces imposed at the mass center of moving platform are defined as

$$\boldsymbol{F}_p = \begin{bmatrix} \boldsymbol{f}_p \\ \boldsymbol{n}_p \end{bmatrix} = \begin{bmatrix} \boldsymbol{f}_e + m_p\boldsymbol{g} - m_p\dot{\boldsymbol{v}} \\ \boldsymbol{n}_e - {}^o\boldsymbol{I}_p\dot{\boldsymbol{\omega}} - \boldsymbol{\omega}\times({}^o\boldsymbol{I}_p\boldsymbol{\omega}) \end{bmatrix} \tag{37}$$

The external force $\boldsymbol{f}_e$ and moment $\boldsymbol{n}_e$ imposed on the moving platform are assumed nonexistent, meaning that $\boldsymbol{f}_e$ and $\boldsymbol{n}_e$ are both set zero. ${}^o\boldsymbol{I}_p = {}^o\boldsymbol{R}_{o'}{}^{o'}\boldsymbol{I}_p{}^o\boldsymbol{R}_{o'}^T$ is the inertia matrix of the moving platform which is expressed in the fixed frame $O-xyz$. $\mathbf{g}$ denotes the gravitational acceleration. It is worthy to note that $\boldsymbol{\omega} = \mathbf{0}$, $\dot{\boldsymbol{\omega}} = \mathbf{0}$, and ${}^o\boldsymbol{R}_{o'} = \boldsymbol{E}_3$, since the fact that this designed proposed 3-PUU PKM is merely provided with three translational capacities.

2. *Applied forces of the struts*. It is clear that the gravitational force is assumed to be the exclusive external force of the rigid struts; hence, the general applied and inertia forces exerted at the mass center of the ith strut in the fixed frame $O-xyz$ is defined as

$$\boldsymbol{F}_i = \begin{bmatrix} \boldsymbol{f}_i \\ \boldsymbol{n}_i \end{bmatrix} = \begin{bmatrix} m_i\boldsymbol{g} - m_i\dot{\boldsymbol{v}}_i \\ -{}^o\boldsymbol{I}_i\dot{\boldsymbol{\omega}}_i - \boldsymbol{\omega}_i\times({}^o\boldsymbol{I}_i\boldsymbol{\omega}_i) \end{bmatrix} \tag{38}$$

where ${}^o\boldsymbol{I}_i = {}^o\boldsymbol{R}_i{}^i\boldsymbol{I}_i{}^o\boldsymbol{R}_i^T$ implies the ith strut's inertia tensor, ${}^i\boldsymbol{I}_i$ represents the ith strut's inertia tensor especially expressed in the local coordinate system $C-x_iy_iz_i$, and m_i denotes the mass of strut i.

3. *Applied forces of the sliders*. Apparently, the sliders posses single translational movement; thus, the applied and inertia forces imposed on the sliders are

$$f_{qi} = (m_{qi}\boldsymbol{g} - m_{qi}\ddot{\boldsymbol{q}}_i)^T\boldsymbol{e} \tag{39}$$

where m_{qi} stands for the mass of slider i.

4. *Applied forces of the motor–coupling–leadscrews*. The particular applied forces and inertia forces exerted at motor–coupling–screw are

$$N_i = \tau_i - (I_{Mi} + I_{Ci} + I_{Li})\ddot{\theta}_i = \tau_i - I_{MCLi}\ddot{\theta}_i \tag{40}$$

where I_{Mi}, I_{Ci}, and I_{Li} are designated as the inertia moment of the motor, coupling, and leadscrew, respectively. τ_i represents the motor's driving torque and $\ddot{\theta}_i$ denotes the angular acceleration of the motor–coupling–leadscrew. The straightforward transition relationship between the motor's rotation and the slider's translation is $\dot{\theta}_i = (2\pi/p_i)\dot{q}_i$ and $\ddot{\theta}_i = (2\pi/p_i)\ddot{q}_i$; p_i denotes the pitch of leadscrew.

Dynamics modeling of the whole system

According to the virtual work principle, the energy generated by these substructure systems can be seamlessly assembled into a thorough interrelated system, that is

$$\delta\boldsymbol{x}_p^T\boldsymbol{F}_p + \sum_{i=1}^{3}\delta\boldsymbol{x}_i^T\boldsymbol{F}_i + \delta\boldsymbol{q}^T\boldsymbol{f}_q + \delta\boldsymbol{\theta}^T\boldsymbol{N} = 0 \tag{41}$$

where $\delta\boldsymbol{q} = [\delta q_1, \delta q_2, \delta q_3]^T$, $\delta\boldsymbol{\theta} = [\delta\theta_1, \delta\theta_2, \delta\theta_3]^T$, $\delta\boldsymbol{\theta} = [\delta\theta_1, \delta\theta_2, \delta\theta_3]^T = diag(2\pi/p_1, 2\pi/p_2, 2\pi/p_3)\delta\boldsymbol{q} = \boldsymbol{A}\delta\boldsymbol{q}$, and $\boldsymbol{f}_q = [f_{q1}, f_{q2}, f_{q3}]^T$, $\boldsymbol{N} = [N_1, N_2, N_3]^T$. $\boldsymbol{F}_i$ and $\boldsymbol{\delta x}_i$ signify the correlative forces and virtual displacements applied to the ith strut, respectively.

Using the LJM defined in equation (29), the crucial mapping relationship between $\delta\mathbf{x}_i$ and $\delta\mathbf{x}_p$ is formulated as follows

$$\delta \boldsymbol{x}_i^T = \delta \boldsymbol{x}_p^T \boldsymbol{J}_{v\omega i}^T \tag{42}$$

Based on the Jacobian matrix defined in equation (23), the corresponding transition relationship between $\delta \boldsymbol{q}$ and $\delta \boldsymbol{x}_p$ is obtained as

$$\delta \boldsymbol{q}^T = \delta \boldsymbol{x}_p^T \boldsymbol{J}^T \tag{43}$$

Substituting equations (40) and (43) into equation (41) and simplifying, the following is obtained

$$\delta \boldsymbol{x}_p^T \left(\boldsymbol{F}_p + \sum_{i=1}^{3} \boldsymbol{J}_{v\omega i}^T \boldsymbol{F}_i + \boldsymbol{J}^T \boldsymbol{f}_q + \boldsymbol{J}^T \boldsymbol{A}^T \boldsymbol{N} \right) = 0 \tag{44}$$

Furthermore, in response to discretional virtual displacement $\delta \boldsymbol{x}_p^T$, equation (44) keeps absolutely maintainable and can be further translated as

$$\boldsymbol{F}_p + \sum_{i=1}^{3} \boldsymbol{J}_{v\omega i}^T \boldsymbol{F}_i + \boldsymbol{J}^T \boldsymbol{f}_q + \boldsymbol{J}^T \boldsymbol{A}^T \boldsymbol{N} = 0 \tag{45}$$

Substituting equation (40) into equation (45), the actuating torques can be computed as follows

$$\boldsymbol{\tau} = -\boldsymbol{A}^{-T} \boldsymbol{J}^{-T} \left(\boldsymbol{F}_p + \sum_{i=1}^{3} \boldsymbol{J}_{v\omega i}^T \boldsymbol{F}_i + \boldsymbol{J}^T \boldsymbol{f}_q \right) + \boldsymbol{I}_{MCL} \ddot{\boldsymbol{\theta}} \tag{46}$$

where

$$\boldsymbol{\tau} = [\tau_1, \tau_2, \tau_3]^T \tag{47}$$

$$\boldsymbol{I}_{MCL} = diag(I_{MCL1}, I_{MCL2}, I_{MCL3}) \tag{48}$$

Simplifying equation (46), the general formulation of dynamics equations expressed in the joint space can be written as

$$\boldsymbol{\tau} = \boldsymbol{D}(\boldsymbol{q}) \ddot{\boldsymbol{q}} + \boldsymbol{C}(\boldsymbol{q}, \dot{\boldsymbol{q}}) \dot{\boldsymbol{q}} + \boldsymbol{G}(\boldsymbol{q}) \tag{49}$$

where

$$\boldsymbol{D}(\boldsymbol{q}) = m_p \boldsymbol{A}^{-T} \boldsymbol{J}^{-T} \boldsymbol{J}^{-1} + \boldsymbol{A}^{-T} \boldsymbol{m}_q + \boldsymbol{I}_{MCL} \boldsymbol{A} + \boldsymbol{A}^{-T} \boldsymbol{J}^{-T} \sum_{i=1}^{3} (m_i \boldsymbol{J}_{vi}^T \boldsymbol{J}_{vi} \boldsymbol{J}^{-1} + \boldsymbol{J}_{\omega i}^{To} \boldsymbol{I}_i \boldsymbol{J}_{\omega i} \boldsymbol{J}^{-1}) \tag{50}$$

$$\boldsymbol{C}(\boldsymbol{q}, \dot{\boldsymbol{q}}) \dot{\boldsymbol{q}} = -m_p \boldsymbol{A}^{-T} \boldsymbol{J}^{-T} \boldsymbol{J}^{-1} \boldsymbol{U} + \boldsymbol{A}^{-T} \boldsymbol{J}^{-T} \sum_{i=1}^{3} \boldsymbol{H}_i \tag{51}$$

$$\boldsymbol{H}_i = \boldsymbol{J}_{wi}^T (\boldsymbol{\omega}_i \times ({}^O \boldsymbol{I}_i \boldsymbol{\omega}_i)) + \frac{l m_i}{2} \boldsymbol{J}_{vi}^T \left(\frac{\tilde{\boldsymbol{w}}_i^2 \boldsymbol{e}}{\boldsymbol{w}_i^T \boldsymbol{e}} + \frac{2\boldsymbol{e}}{\boldsymbol{w}_i^T \boldsymbol{e}} - \boldsymbol{w}_i \right) - (m_i \boldsymbol{J}_{vi}^T \boldsymbol{J}_{vi} + \boldsymbol{J}_{wi}^{T\,O} \boldsymbol{I}_i \boldsymbol{J}_{wi}) \boldsymbol{J}^{-1} \boldsymbol{U} - \boldsymbol{J}_{wi}^{T\,O} \boldsymbol{I}_i \frac{\tilde{\boldsymbol{w}}_i \boldsymbol{e}}{\boldsymbol{w}_i^T \boldsymbol{e}} \tag{52}$$

$$\boldsymbol{G}(\boldsymbol{q}) = -\boldsymbol{A}^{-T} \boldsymbol{J}^{-T} \left\{ m_p \boldsymbol{g} + \sum_{i=1}^{3} \boldsymbol{J}_{v\omega i}^T \begin{bmatrix} m_i \boldsymbol{g} \\ \boldsymbol{0} \end{bmatrix} + \boldsymbol{J}^T \left[m_{q1} \boldsymbol{g}^T \boldsymbol{e}, m_{q2} \boldsymbol{g}^T \boldsymbol{e}, m_{q3} \boldsymbol{g}^T \boldsymbol{e} \right]^T \right\} \tag{53}$$

$$\boldsymbol{m}_q = diag(m_{q1}, m_{q2}, m_{q3}) \tag{54}$$

where $\boldsymbol{D}(\boldsymbol{q}) \ddot{\boldsymbol{q}}$ stands for the inertial term, $\boldsymbol{C}(\boldsymbol{q}, \dot{\boldsymbol{q}}) \dot{\boldsymbol{q}}$ denotes the nonlinear term including centrifugal and Coriolis forces, and $\boldsymbol{G}(\boldsymbol{q})$ represents the gravitational force. The accurate dynamics modeling by the virtual work principle plays a significantly important role in undertaking the quantitative analysis and critical assessment that pertains to systemic dynamics property between end-effector's movement and joints' torque, while simultaneously providing a vital premise for the practical trajectory planning.

Parameterization of trajectory planning based on the minimum-jerk strategy

Rational running trajectory is the foundation of preeminent kinematics property of PKMs, and the quality of trajectory planning algorithm directly affects the dynamics performance of PKMs. As a noticeable drawback, high jerk value during the entire trajectory can decrease the motion precision, excite the dominating vibration, and even break the structure life. Therefore, the minimum-jerk trajectory planning approach aiming to minimize the jerk value of motion period is recommended to regulate the driving joints' motion functions to make sure all joints pass through the corresponding joints' positions simultaneously and smoothly.[38,39] Considering the actual control system effects directly on the active joints, trajectory planning executed in joint space is more convenient and easier to guarantee the continuity and smoothness of joints' angular movement curves than that in operation space. Hence, this minimum-jerk trajectory planning approach is implemented by the desired joints' via-positions which are transformed from the path points in operation space through inverse kinematics calculation.

Interpolation functions based on piecewise quintic polynomials

Figure 6 shows a typical geometric description of the sequence of via-points in Cartesian space (i.e. operation space). The fundamental objective and mission of trajectory planning, as stated previously, are to confirm a stringent and reasonable trajectory between the designated starting point and the specific destination within the reachable workspace.[40] In general, the original trajectory in Cartesian space is continuous and discretized into $(n-1)$ segments by the requisite n via-points. First,

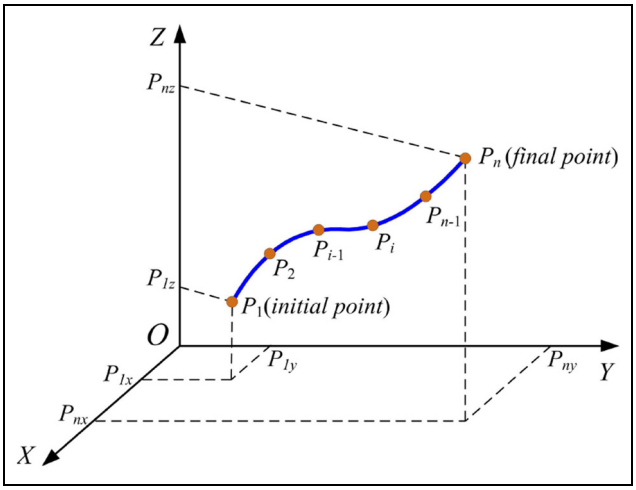

Figure 6. Via-points in Cartesian space.

the corresponding kth joint angular position knots are defined as $Q_{k,i}$ that obtained through inverse kinematics mapping of the given geometric path. Without loss of generality, we allow $t_1 < t_2 < \cdots < t_{n-1} < t_n$ to be an ordered time sequence and define $h_i = t_{i+1} - t_i$ as the corresponding time interval; thus, the total execution time is $\sum_{i=1}^{n-1} h_i$. The lowest order polynomials to guarantee the smoothness of jerk profile at the sequence of via-points are quintic polynomials of which jerk profile is quadratic polynomials and with C^2 continuity. Thus, to guarantee the demanding continuity and smoothness property of variation curves of separate joint's angular position, velocity, and acceleration, the sequences of via-points denoted in joint space need to be interpolated by the discretized piecewise quintic polynomials. The ith interpolation function $Q_{k,i}(t)$ connecting the point i and the point $(i+1)$ for the kth joint can be expressed as

$$Q_{k,i}(t) = \sum_{j=0}^{5} u_{ki,j} t^j \tag{55}$$

where $t \in [t_i, t_{i+1}]$. Consequently, in response to the aforementioned position profile, implementing the first-, second-, and third-order derivatives regarding time can immediately yield the corresponding velocity $\dot{Q}_{k,i}(t)$, acceleration $\ddot{Q}_{k,i}(t)$, and jerk $\dddot{Q}_{k,i}(t)$ in the kth coordinate direction relative to the ith time interval, that is

$$\dot{Q}_{k,i}(t) = \sum_{j=0}^{4} (j+1) u_{ki,(j+1)} t^j \tag{56}$$

$$\ddot{Q}_{k,i}(t) = \sum_{j=0}^{3} (j+1)(j+2) u_{ki,(j+2)} t^j \tag{57}$$

$$\dddot{Q}_{k,i}(t) = \sum_{j=0}^{2} (j+1)(j+2)(j+3) u_{ki,(j+3)} t^j \tag{58}$$

Obviously, the jerk is a quadratic function of time, it has a continuous second derivative ("C^2 continuity") and cannot produce severe step change. To meet high-level continuity and smoothness requirements, the position, velocity, acceleration and jerk at endpoint of ith time interval must equal to the position, velocity, acceleration, and jerk at starting point of $(i+1)$th time interval, respectively. Thus, equations (55)–(57) can be written as a vector-matrix differential equation, specifically

$$\begin{bmatrix} 1 & 0 & 0 & 0 & 0 & 0 \\ 0 & 1 & 0 & 0 & 0 & 0 \\ 0 & 0 & 2 & 0 & 0 & 0 \\ 1 & t_{i+1} & t_{i+1}^2 & t_{i+1}^3 & t_{i+1}^4 & t_{i+1}^5 \\ 0 & 1 & 2t_{i+1} & 3t_{i+1}^2 & 4t_{i+1}^3 & 5t_{i+1}^4 \\ 0 & 0 & 2 & 6t_{i+1} & 12t_{i+1}^2 & 20t_{i+1}^3 \end{bmatrix} \begin{bmatrix} u_{ki,0} \\ u_{ki,1} \\ u_{ki,2} \\ u_{ki,3} \\ u_{ki,4} \\ u_{ki,5} \end{bmatrix} = \begin{bmatrix} Q_{k,i} \\ \dot{Q}_{k,i} \\ \ddot{Q}_{k,i} \\ Q_{k,i+1} \\ \dot{Q}_{k,i+1} \\ \ddot{Q}_{k,i+1} \end{bmatrix} \tag{59}$$

Solving equation (59), the coefficients of equation (55) are obtained, namely

$$\begin{cases} u_{ki,0} = Q_{k,i} \\ u_{ki,1} = \dot{Q}_{k,i} \\ u_{ki,2} = \frac{\ddot{Q}_{k,i}}{2} \\ u_{ki,3} = \frac{20(Q_{k,i+1} - Q_{k,i}) - (12\dot{Q}_{k,i} + 8\dot{Q}_{k,i+1})h_i - (3\ddot{Q}_{k,i} - \ddot{Q}_{k,i+1})h_i^2}{2h_i^3} \\ u_{ki,4} = \frac{30(Q_{k,i} - Q_{k,i+1}) + (16\dot{Q}_{k,i} + 14\dot{Q}_{k,i+1})h_i - (3\ddot{Q}_{k,i} + 2\ddot{Q}_{k,i+1})h_i^2}{2h_i^4} \\ u_{ki,5} = \frac{12(Q_{k,i+1} - Q_{k,i}) - 6(\dot{Q}_{k,i} + \dot{Q}_{k,i+1})h_i - (\ddot{Q}_{k,i} - \ddot{Q}_{k,i+1})h_i^2}{2h_i^5} \end{cases} \tag{60}$$

Strict and necessary constraints

In particular, the total execution time of our minimum-jerk trajectory planning strategy is set as a specific constraint. Arising from the proposed minimum-jerk trajectory planning algorithm imposed upon the 3-PUU PKM, all strict and necessary constraints consist of (1) meeting the predefined state conditions at the initial and ultimate time; (2) fulfilling the definite continuity and smoothness requirements with regard to position, velocity, acceleration, and jerk for specific relevant via-points; (3) satisfying the explicit kinematics restraints; (4) abiding by the specific dynamics bounds;

and (5) subjecting to the limitation of total execution time.

1. *Initial and ultimate time constraints*. Consistent with the initial and ultimate time prerequisites, the joints' angular velocity, acceleration, and jerk at initial and final time are undoubtedly guaranteed to be zero simultaneously as follows

$$\begin{cases} Q_{k,0} = q_{k0}, Q_{k,n} = q_{kn} \\ \dot{Q}_{k,0} = \dot{q}_{k0} = 0, \dot{Q}_{k,n} = \dot{q}_{kn} = 0 \\ \ddot{Q}_{k,0} = \ddot{q}_{k0} = 0, \ddot{Q}_{k,n} = \ddot{q}_{kn} = 0 \\ Q_{k,0} = q_{k0} = 0, Q_{k,n} = q_{kn} = 0 \end{cases} \tag{61}$$

2. *Continuity constraints*. Particularly, the main challenge facing trajectory planner is to achieve the essential continuity and smoothness requirements; therefore, the joints' angular position, velocity, acceleration, and jerk at every inter-knot must satisfy the following continuity constraints, namely

$$\begin{cases} Q_{k,i}(t_{i+1}) = Q_{k,i+1}(t_{i+1}) = q_{ki} & \forall k, i \\ \dot{Q}_{k,i}(t_{i+1}) = \dot{Q}_{k,i+1}(t_{i+1}) & \forall k, i \\ \ddot{Q}_{k,i}(t_{i+1}) = \ddot{Q}_{k,i+1}(t_{i+1}) & \forall k, i \\ Q_{k,i}(t_{i+1}) = Q_{k,i+1}(t_{i+1}) & \forall k, i \end{cases} \tag{62}$$

3. *Kinematics constraints*. Apparently, kinematics constraints concern that the joints' angular velocity, acceleration, and jerk at every inter-knot should not exceed the given specific maximum values

$$\begin{cases} |\dot{Q}_{k,i}| \leqslant VC_k & \forall k, i \\ |\ddot{Q}_{k,i}| \leqslant AC_k & \forall k, i \\ |\dddot{Q}_{k,i}| \leqslant JC_k & \forall k, i \end{cases} \tag{63}$$

where VC_k, AC_k, and JC_k represent the kth joint's velocity bound, acceleration bound, and jerk bound, respectively.

4. *Dynamics constraints*. The torque constraint of actuating joint based on its motor's driving capacity has to be taken into account when the appointed trajectory is reasonably processed, that is

$$|\boldsymbol{\tau}_{k,i}| \leqslant \tau C_k \quad \forall k, i \tag{64}$$

where τC_k denotes the kth joint's active torque limitation.

5. *Total execution time constraint*. Generally, as an additional requirement, the total traveling time allocated to the confirmed operation should be less than the given execution time in order to boost the operation efficiency and productivity, thereby

$$T = \sum_{i=1}^{n} h_i \leqslant TC \tag{65}$$

where TC is the artificial traveling time bound.

Objective function

For sophisticated industrial operations, the smoother trajectories are always preferred to the rougher ones; smoother trajectories usually ensure smaller vibration deformation and higher positioning accuracy. Since limiting the maximum jerk value of the entire trajectory is of considerable benefits—reducing structure wear, suppressing motivated vibration, enhancing smoothness degree, and raising tracking accuracy—the maximum absolute value of each individual joint's angular jerk function within every specific segment needs to be minimized. Hence, the objective function we adopt is given as follows

$$min\ max|\dddot{Q}_{k,i}(t)|, i = 1, \ldots, n;\ k = 1, \ldots, m \tag{66}$$

where n is the number of total via-points (including the starting point and the destination) and m is the number of driving joints. The indispensable coefficients u_{kij} of interpolation functions for joints' angular position are viewed as the independent design variables. Complying fully with the multiple fundamental constraints, we can perform the minimum-jerk trajectory planning with a path parameterized by piecewise quintic polynomials. The coefficients u_{kij} of joint's angular position profile are obtained by $\dot{Q}_{k,i}$, $\ddot{Q}_{k,i}$, and h_i through equation (60). For a m-joint n-knot trajectory planning problem featuring minimum-jerk, the velocity and acceleration at starting point and endpoint ($\dot{Q}_{1,i}$, $\ddot{Q}_{1,i}$, $\dot{Q}_{m,i}$, $\ddot{Q}_{m,i}$) are first set zero upon requisite constraints, and its unknown velocity and acceleration at subsequent inter via-points are primary design factors. Besides, the $(n-1)$ time internals are needed to be optimized and identified. Thus, the number of total design variables is $[m \times 2 \times (n-1) + (n-1)]$.

Optimization method

Figure 7 illustrates an overview of the thorough minimum-jerk trajectory planning procedure aiming at the 3-PUU PKM. From the perspective of mathematics, the complex trajectory planning matter of PKM is further converted into a traditional constrained nonlinear multivariable optimization problem. The objective of this particular optimization problem is to minimize the maximum absolute value of joints' angular jerk subject to the aforementioned continuity constraints, kinematics constraints, dynamics constraints, and execution time constraints. To solve the optimal solution of the constrained multivariable objective function, the minimum-jerk trajectory generation

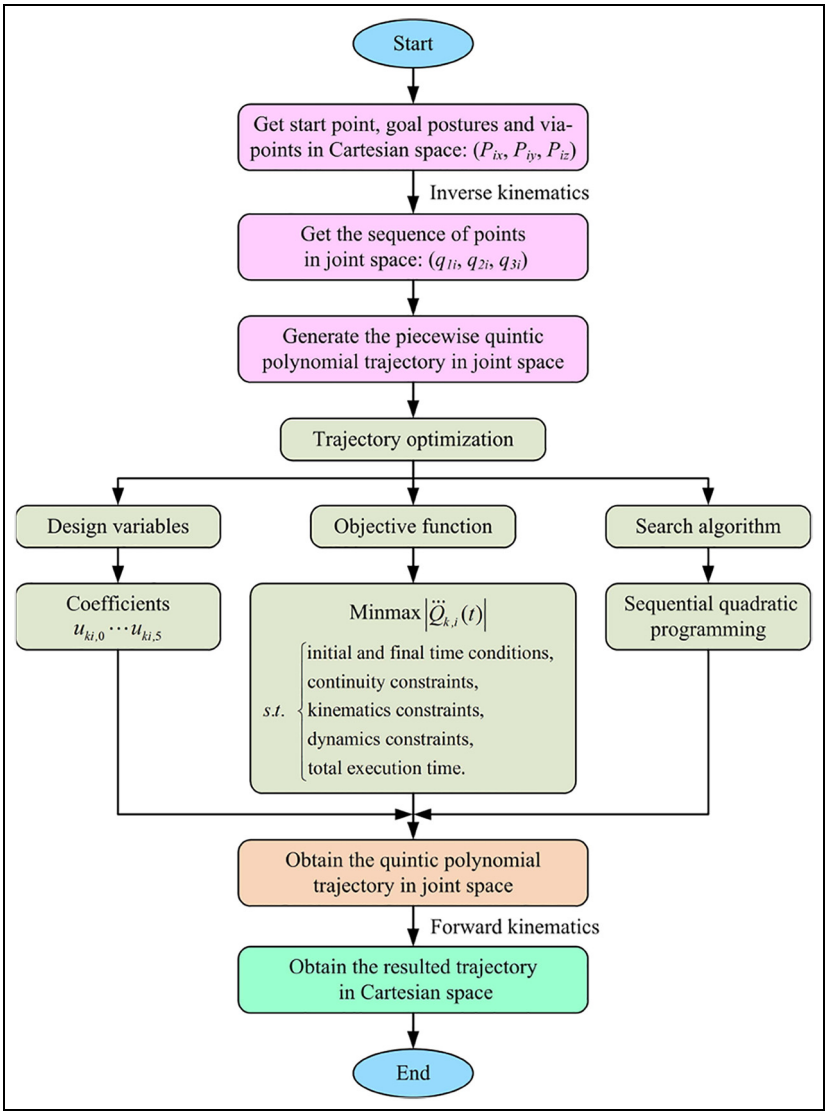

Figure 7. Flowchart of the proposed trajectory planning.

strategy presented herein has to resort to the professional computing software—MATLAB, which is integrated many distinguished and reliable calculation algorithms including sequential quadratic programming (SQP) algorithm, genetic algorithm (GA), and particle swarm optimization (PSO) algorithm. Among highly efficient methods to deal with general constrained optimization problems, the SQP approach is filled with significant advantages of solving large-scale complex problems and capable of relatively fast convergence rate; thus, we employ familiar SQP algorithm embedded in the *fmincon* function to fully address the minimum-jerk trajectory planning problem.

Numerical simulation

The 3-PUU parallel kinematic manipulator is an automatic operation mechanism that can grasp and transport objects or operation tools accurately and flexibly according to the fixed procedures. To intuitively observe and evaluate the concrete characteristics of the presented minimum-jerk trajectory planning approach, two different but representative examples—an inverted U-shaped trajectory intensively applied for pick-and-place operations and a closed spatial circle trajectory widely used for painting or spraying operations—are simulated and discussed in this section.

Case I: pick-and-place operation application

By investigating the handling process of practical production line, the most frequently used trajectory of pick-and-place operation is a bow-shaped trajectory,[41] which is approximately considered as an inverted U-shaped trajectory. As depicted in Figure 8, the red solid

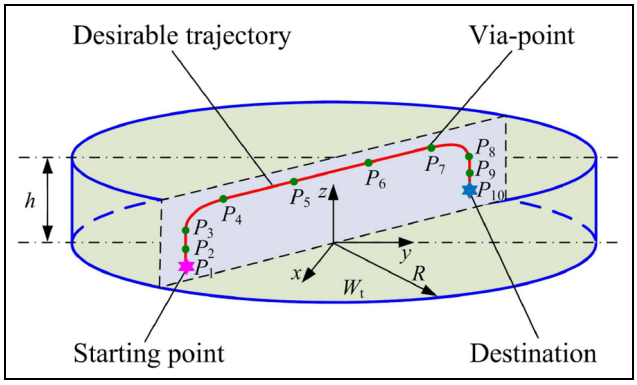

Figure 8. The presupposed pick-and-place operation trajectory.

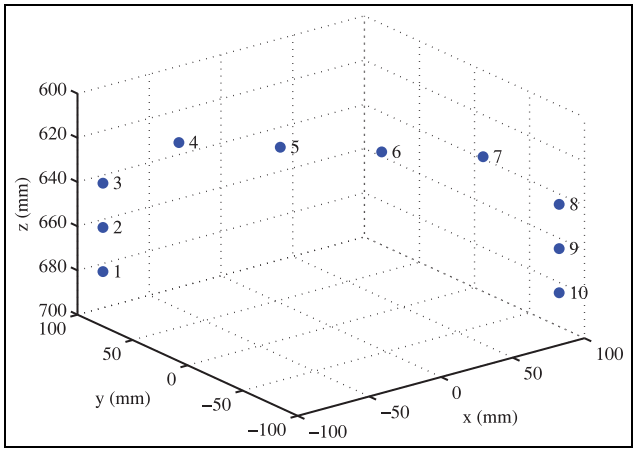

Figure 9. The via-points of pick-and-place operation trajectory.

line in the dexterous workspace (W_t) of 3-PUU PKM denotes the presupposed inverted U-shaped trajectory for a flexible pick-and-place application. As illustrated in Figure 9, we select 10 predefined points ($P_1 - P_{10}$) in Cartesian space as the key via-points for the inverted U-shaped trajectory sample. To ensure the joints' motion trajectories are planned definitely in joint space, these given via-points need to be converted into the corresponding joints' angular position knots in joint space through inverse kinematics computation. All indispensable prototype parameters of the 3-PUU PKM are reported concisely in Table 1. Its orderly sequence of via-points in Cartesian space and joints' angular position knots in joint space is listed in Table 2. The necessary kinematics and dynamics constraints of the 3-PUU PKM are recorded in Table 3. The allowable joints' angular velocity limitation VC_k is 0.5 m/s, the joints' angular acceleration limitation AC_k is 1.2 m/s^2, the joints' angular jerk limitation JC_k is 5 m/s^3, and the joints' torque limitation τC_k is 10 N m. In addition, the total traveling time bound TC is artificially set to 5 s

Table 1. Physical parameters of the 3-PUU PKM.

Symbol	Description	Value	Unit
s	Radius of the moving platform	0.070	m
S	Radius of the fixed base	0.370	m
l	Strut's length	0.450	m
d	Distance from C_i to leadscrew	0.070	m
R	Radius of the task workspace	0.080	m
h	Height of the task workspace	0.200	m
m	Mass of the moving platform	3.500	kg
m_i	Mass of the strut	0.720	kg
m_{qi}	Mass of the slider	1.377	kg
I_{Mi}	Motor's inertia moment	1.4e–4	N/m^2
I_{Ci}	Coupling's inertia moment	1.3e–5	N/m^2
I_{Li}	Leadscrew's inertia moment	1.1e–4	N/m^2
p_i	Leadscrew's pitch	0.010	m
g	Gravitational acceleration	9.807	m/s^2

PUU: prismatic-universal-universal; PKM: parallel kinematic manipulator.

Table 2. The via-points of the pick-and-place operation trajectory.

Knots	Cartesian space (mm)			Joint space (mm)		
	x	y	z	Joint 1	Joint 2	Joint 3
1	−90	90	680	376.68	244.16	336.13
2	−90	90	660	356.68	224.16	316.13
3	−90	90	640	336.68	204.16	296.13
4	−60	60	620	281.18	195.62	256.27
5	−20	20	620	246.40	218.29	238.64
6	20	−20	620	222.51	250.90	229.91
7	60	−60	620	207.69	296.43	229.48
8	90	−90	640	221.91	362.79	254.57
9	90	−90	660	241.91	382.79	274.57
10	90	−90	680	261.91	402.79	294.57

Table 3. Kinematics and dynamics constraints of the 3-PUU PKM.

Constraints values		Joint 1	Joint 2	Joint 3
Kinematics constraints	VC_k (m/s)	0.5	0.5	0.5
	AC_k (m/s^2)	1.2	1.2	1.2
	JC_k (m/s^3)	5.0	5.0	5.0
Dynamics constraints	$\lvert\tau\rvert_{max}$ (N m)	10	10	10

PUU: prismatic-universal-universal; PKM: parallel kinematic manipulator.

in this case. Finally, in the major parameter options of *fmincon* function, the approved maximum number of iterations "MaxIter" is set 100, and the authorized maximum number of function evaluations "MaxFunEvals" is set 5000.

Conforming to the specifically designed procedure for minimum-jerk trajectory planning, the total

Table 4. Optimized time intervals of the pick-and-place trajectory.

Intervals (s)	h_1	h_2	h_3	h_4	h_5
	0.738	0.238	0.588	0.370	0.388
Intervals (s)	h_6	h_7	h_8	h_9	T
	0.623	0.799	0.267	0.756	4.767

Table 5. Resulting values of the pick-and-place trajectory.

Values		Joint 1	Joint 2	Joint 3
Maximum values	$\|V\|_{max}$ (m/s)	0.101	0.101	0.090
	$\|A\|_{max}$ (m/s^2)	0.181	0.279	0.178
	$\|J\|_{max}$ (m/s^2)	1.010	3.102	0.952
	$\|\tau\|_{max}$ (N m)	2.064	3.141	1.996
Mean values	$\|V\|_{mea}$ (m/s)	0.049	0.054	0.037
	$\|A\|_{mea}$ (m/s^2)	0.077	0.095	0.077
	$\|J\|_{mea}$ (m/s^2)	0.344	0.516	0.348
	$\|\tau\|_{mea}$ (N m)	0.872	1.078	0.873

traveling time after massive computation in MATLAB environment is 4.767 s, as can be seen from Table 4. The four longest time intervals are h_1 (from P_1 to P_2), h_3 (from P_3 to P_4), h_7 (from P_7 to P_8), and h_9 (from P_9 to P_{10}). As summarized in Table 5, the maximum of the absolute value of joints' velocity, acceleration, jerk, and torque are 0.101 m/s, 0.279 m/s^2, 3.102 m/s^3, and 3.141 N m, respectively, suggesting that none of terms oversteps the fundamental limitations of kinematics and dynamics bounds. Besides, the mean of the absolute value of joints' velocity, acceleration, jerk, and torque are 0.054 m/s, 0.095 m/s^2, 0.516 m/s^3, and 1.078 N m, respectively. Note that the maximum velocity, acceleration, jerk, and torque occur on Joint 2. Hence, with respect to this inverted U-shaped trajectory, Joint 2 needs to be paid more attention and further strengthened than Joints 1 and 3. Figure 10(a)–(e) shows the associated joints' position, velocity, acceleration, jerk, and torque profiles corresponding to the available optimal solution. The red solid line depicted in Figure 10(f) exhibits the generated valid trajectory of moving platform by the forward position transformation analyzed above. It is clear that the generated Cartesian trajectory strictly goes through all the predefined via-points, approximates the assumed inverted U-shaped path, and satisfies all the specific constraints. Especially, there are no fierce step changes in joints' position, velocity, and acceleration profiles. To sum up, the minimum-jerk trajectory planning strategy enables the profiles of joints' position, velocity, acceleration, jerk, and torque to be characterized by excellent continuity and pronounced smoothness relating to the inverted U-shaped trajectory.

Case II: closed circle application

This section mainly describes the simulation results of the presented minimum-jerk trajectory planning strategy for a particularly circle trajectory in Cartesian space. The presupposed closed circle trajectory for painting operation is a red dash-dotted line displayed in Figure 11. We choose 11 definite points, $P_1 - P_{11}$, as the important via-points on the circle trajectory where the first point P_1 coincides exactly with the last point P_{11}. As listed in Table 6, the sequence of joints' angular position knots corresponding for the prescribed points in Cartesian space are calculated using inverse kinematics transformation. The kinematics and dynamics constraints with regard to the circle trajectory are as the same as the constraints for the inverted U-shaped trajectory. Likewise, the limitation of total traveling time TC is also set 5 s.

The process implementation of Case II, circle trajectory planning, is closely followed with Case I where the major parameter options of *fmincon* function remain constant to resolve the constrained optimization problem. As can be seen from Table 7, the optimized total traveling time just equals to the setting time bound under the satisfied continuity and smoothness requirements. The four longest time intervals are h_1 (from P_1 to P_2), h_5 (from P_5 to P_6), h_6 (from P_6 to P_7), and h_{10} (from P_{10} to P_{11}). As summarized in Table 8, the maximum of the absolute value of joints' angular velocity, acceleration, jerk, and torque are 0.254 m/s, 0.730 m/s^2, 2.808 m/s^3, and 8.246 N m, respectively, indicating that no associated term oversteps the principal limitations of kinematics and dynamics restrictions. Besides, the mean of the absolute value of joints' angular velocity, acceleration, jerk, and torque are 0.111 m/s, 0.241 m/s^2, 0.709 m/s^3, and 2.725 N m, respectively. Figure 12(a)–(e) reveals the simulated joints' angular position, velocity, acceleration, jerk, and torque profiles resulted from the corresponding ultimate optimal solution. Utilizing the forward position transformation of input joints' angular position functions, the visible trajectory of moving platform is exhibited in Figure 12(f). It is important to note that the generated spatial circle trajectory strictly goes through all the predefined via-points, approximates the predefined closed circle path, and satisfies the specific restrictive conditions. The profiles of joint angular position, velocity, acceleration, jerk, and torque are characterized with excellent continuity; there are no fierce step changes in joint angular position, velocity, and acceleration profiles. To some extent, the peak and tendency of the angular velocity, acceleration, jerk, and torque variations of these independent joints are relatively close. Contrasting to simulation results of the inverted U-shaped trajectory, no particular attention needs to be given to Joint 2 for the closed circle trajectory, suggesting that the choice and

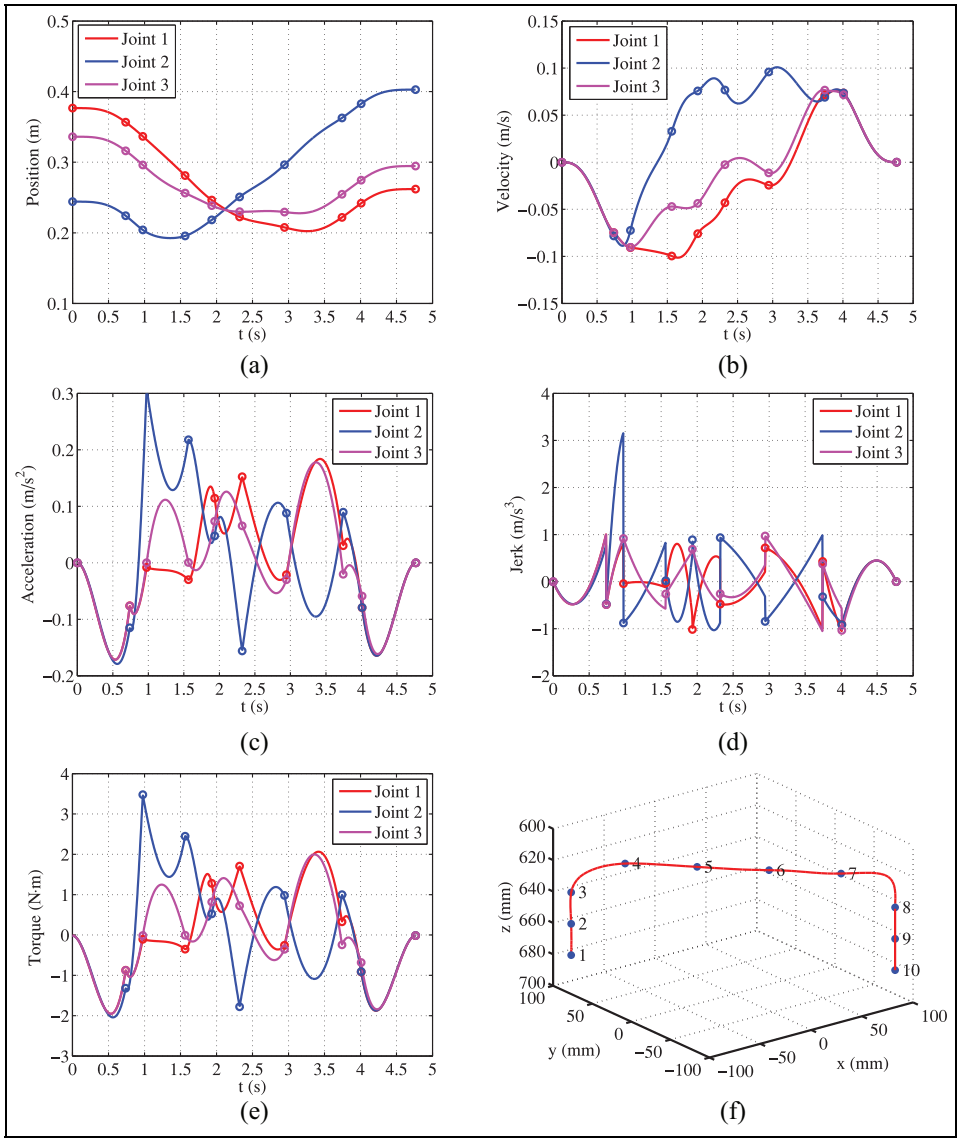

Figure 10. The resulted profiles related to the pick-and-place operation trajectory: (a) joint position, (b) joint velocity, (c) joint acceleration, (d) joint jerk, (e) joint torque, and (f) resulted trajectory.

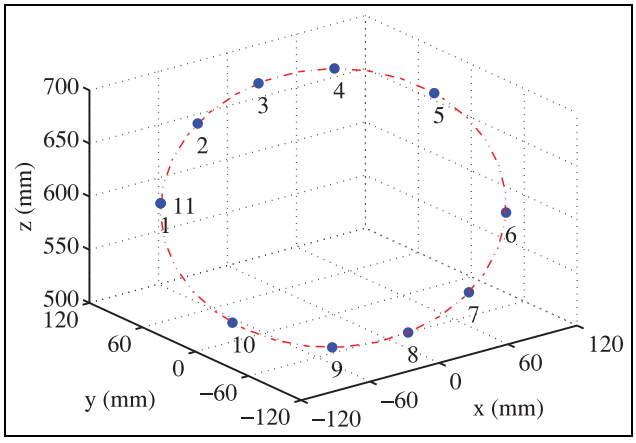

Figure 11. The presupposed circle trajectory in Cartesian space.

determination of driving motor can be influenced by the quality of practical trajectory. According to the discussions reported in Cases I and II, the results of simulation suggest that the established joints' jerk profiles are undoubtedly continuous, and the joints' torque profiles are clearly smooth. The proposed minimum-jerk trajectory planning strategy for the 3-PUU PKM can provide a desirable trajectory with great continuity and pleasing smooth performance. By virtue of this minimum-jerk approach for trajectory planning, we can expect a steady decline in the number of discontinuities and unsmoothness suffered by the inapposite motion trajectory. Moreover, the proposed minimum-jerk trajectory planning approach has advantages of strong reliability, high flexibility, and simple

Table 6. Trajectory via-points of the circle trajectory.

Knots	Operation space (mm)			Joint space (mm)		
	x	y	z	Joint 1	Joint 2	Joint 3
1	−86	83.66	597.66	288.39	163.71	248.87
2	−43	97.74	654.74	310.62	222.28	324.36
3	0	84.85	684.85	307.49	265.09	355.31
4	43	54.74	697.74	292.11	301.92	361.50
5	86	−2.34	683.66	257.33	335.11	332.45
6	86	−83.66	602.34	184.29	315.81	216.66
7	43	−97.74	545.26	147.80	246.31	136.30
8	0	−84.85	515.15	137.79	185.61	95.39
9	−43	−54.74	502.26	148.74	137.79	82.20
10	−86	2.34	516.34	195.97	112.72	115.03
11	−86	83.66	597.66	288.39	163.71	248.87

Table 7. Optimized time intervals of the circle trajectory.

Intervals (s)	h_1	h_2	h_3	h_4	h_5	h_6
	1.027	0.229	0.225	0.347	0.583	0.455
Intervals (s)	h_7	h_8	h_9	h_{10}	T	
	0.255	0.212	0.307	1.359	5.0	

Table 8. Resulting values of the circle trajectory.

Values		Joint 1	Joint 2	Joint 3
Maximum values	$\lvert V\rvert_{max}$ (m/s)	0.178	0.254	0.224
	$\lvert A\rvert_{max}$ (m/s^2)	0.496	0.672	0.730
	$\lvert J\rvert_{max}$ (m/s^3)	2.529	2.808	2.799
	$\lvert\tau\rvert_{max}$ (N m)	5.598	7.588	8.246
Mean values	$\lvert V\rvert_{mea}$ (m/s)	0.069	0.090	0.111
	$\lvert A\rvert_{mea}$ (m/s^2)	0.144	0.208	0.241
	$\lvert J\rvert_{mea}$ (m/s^3)	0.631	0.651	0.709
	$\lvert\tau\rvert_{mea}$ (N m)	1.630	2.351	2.725

implementation. Additionally, as a supplementary statement, it is important to point out that the optimized result computed by *fmincon* function is sensitive to the initial solution. The choice of proper initial value has slightly influence on the final simulation results; in other words, an inapposite choice may disturb the execution time, the convergence of iterative algorithm, and the final simulation results. Thus, the determination of suitable initial solution is also an important factor needed to be serious consideration.

Conclusion

Limiting the maximum jerk of manipulator's trajectory contributes to suppressing the vibration induced by the dominating vibratory mode, reducing the structure wear, and improving trajectory smoothness and tracking accuracy. This article focuses on taking jerk minimization as the most important consideration for trajectory planning issue of parallel manipulators. In the presence of specific kinematics constraints, dynamics constraints, and execution time constraints, this article presents a minimum-jerk trajectory planning approach for smooth trajectory generation applied to the translational 3-PUU PKM. Despite a little computational cost, the relatively comprehensive smoothness performance of the proposed minimum-jerk trajectory planning strategy is clearly described and borne out by two hypothesized representative examples. The following conclusions are drawn:

1. The complete kinematics characteristics of this vertical 3-PUU PKM are thoroughly analyzed. In particular, there exists a reliable unique solution in the forward position analysis aspect of the remarkable 3-PUU parallel mechanism structure. Relying on the LJMs and virtual work principle, the complicated dynamics model is formulated without neglecting the inertial and gravitational effects of the struts.
2. The straightforward objective of the proposed minimum-jerk trajectory planning is minimizing the maximum absolute value of joints' angular jerk profile relating to satisfy strict and necessary constraints of initial time, final time, continuity, kinematics, dynamics, and execution time. The discretized piecewise fifth-order

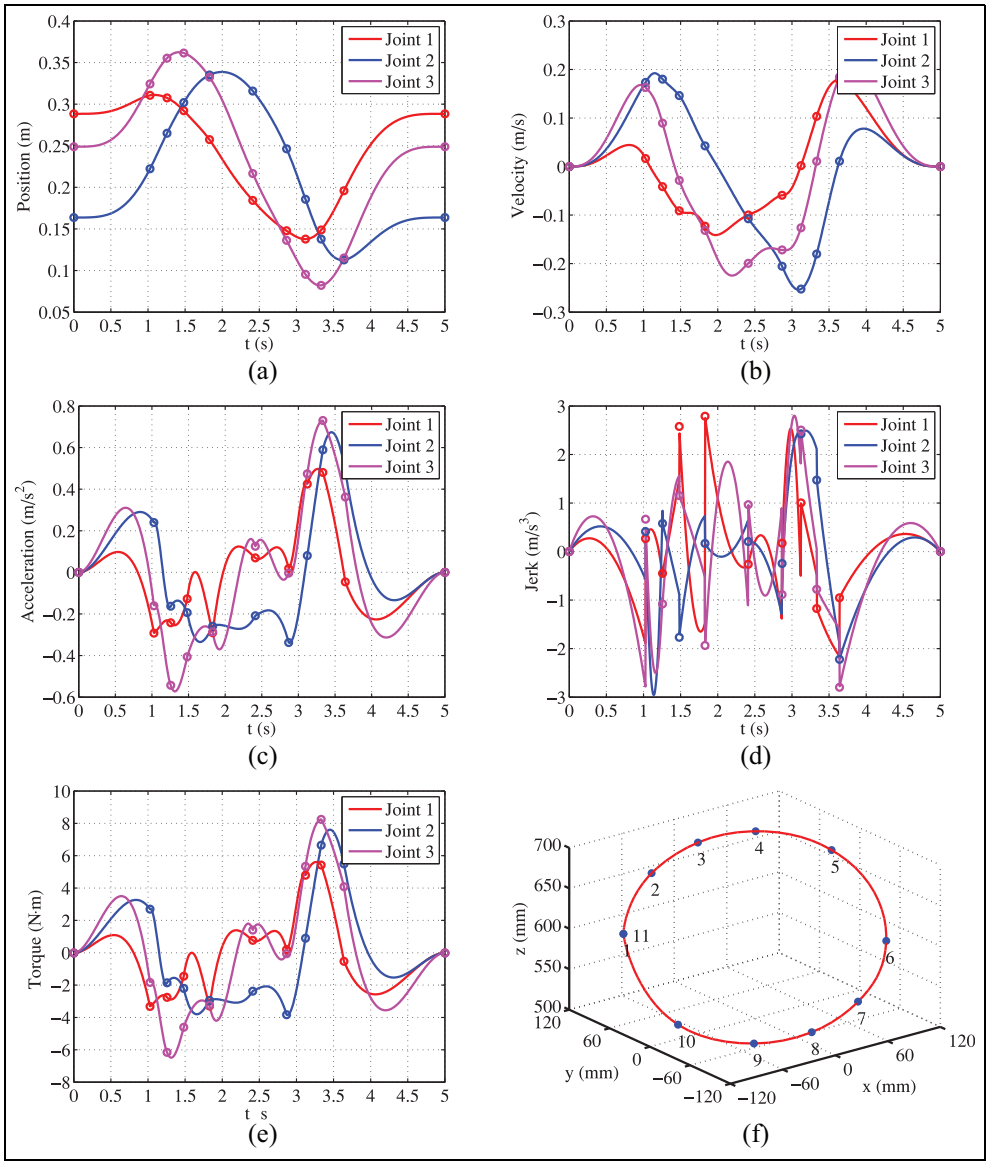

Figure 12. The resulted profiles related to the circle trajectory: (a) joint position, (b) joint velocity, (c) joint acceleration, (d) joint jerk, (e) joint torque, and (f) resulted trajectory.

polynomials are utilized to interpolate the sequence of joints' angular position knots which are transformed from a series of predefined via-points by inverse kinematics mapping.

3. Using SQP algorithm available in MATLAB, empirical simulation results for the inverted U-shaped trajectory and closed circle trajectory demonstrate that the planned trajectory stemming from the minimum-jerk trajectory planning strategy is of significant continuity and pronounced smoothness. In conclusion, this efficient and feasible methodology has substantial contribution for high-level smoothness requirements particularly applicable to the general parallel manipulators.

Acknowledgements

The authors would like to acknowledge the anonymous reviewers for their insightful comments and suggestions.

Declaration of conflicting interests

The author(s) declared no potential conflicts of interest with respect to the research, authorship, and/or publication of this article.

Funding

The author(s) disclosed receipt of the following financial support for the research, authorship, and/or publication of this article: This work was supported by the National Natural Science Foundation of China (grant nos 51575544, 51275353),

HuXiang High-Level Talent Project of Hunan Province (grant no. 2019RS1066), Education Department of Hunan Province (grant no. 19C1520), and the Macao Science and Technology Development Fund (grant no. 110/2013/A3).

ORCID iD

Song Lu https://orcid.org/0000-0003-3414-0362

References

1. Zhang D and Gao Z. Hybrid head mechanism of the groundhog-like mine rescue robot. *Robot Cim: Int Manuf* 2011; 27: 460–470.
2. Liu XJ and Wang JS. A new methodology for optimal kinematic design of parallel mechanisms. *Mech Mach Theory* 2007; 42: 1210–1224.
3. Lu S, Li YM and Ding BX. Multi-objective dimensional optimization of a 3-DOF translational PKM considering transmission properties. *Int J Automat Comput* 2019; 16: 748–760.
4. Ni YB, Jia SL, Zhang ZW, et al. A manufacturing-oriented error modelling method for a hybrid machine tool based on the 3-PRS parallel spindle head. *Adv Mech Eng*. Epub ahead of print 6 May 2019. DOI: 10.1177/1687814019848902
5. Mei JP, Zhang X, Zhang JW, et al. Optimization design using a global and comprehensive performance index and angular constraints in a type of parallel manipulator. *Int J Adv Robot Syst*. Epub ahead of print 12 July 2018. DOI: 10.1177/1687814018787068
6. Huang T, Li ZX, Li M, et al. Conceptual design and dimensional synthesis of a novel 2-DOF translational parallel robot for pick-and-place operations. *J Mech Des: T ASME* 2004; 126: 449–455.
7. Zhao YJ and Gao F. Dynamic performance comparison of the 8PSS redundant parallel manipulator and its non—redundant counterpart—the 6PSS parallel manipulator. *Mech Mach Theory* 2009; 44: 991–1008.
8. Dalvand MM and Shirinzadeh B. Motion control analysis of a parallel robot assisted minimally invasive surgery/microsurgery system (PRAMiSS). *Robot Cim: Int Manuf* 2013; 29: 318–327.
9. Li YM and Xu QS. Design and development of a medical parallel robot for cardiopulmonary resuscitation. *IEEE/ASME T Mech* 2007; 12: 265–273.
10. Chen QZ, Zhang CR, Ni HP, et al. Trajectory planning method of robot sorting system based on S-shaped acceleration/deceleration algorithm. *Int J Adv Robot Syst*. Epub ahead of print 22 November 2018. DOI: 10.1177/1729881418813805
11. Zha XF. Optimal pose trajectory planning for robot manipulators. *Mech Mach Theory* 2002; 37: 1063–1086.
12. Boryga M and Graboś A. Planning of manipulator motion trajectory with higher-degree polynomials use. *Mech Mach Theory* 2009; 44: 1400–1419.
13. Yang P, Tang K, Lozano JA, et al. Path planning for single unmanned aerial vehicle by separately evolving waypoints. *IEEE T Robot* 2015; 31: 1130–1146.
14. Biagiotti L and Melchiorri C. *Trajectory planning for automatic machines and robots*. Berlin: Springer-Verlag, 2008.
15. Gasparetto A and Zanotto V. A technique for time-jerk optimal planning of robot trajectories. *Robot Cim: Int Manuf* 2008; 24: 415–426.
16. Berglund T, Brodnik A, Jonsson H, et al. Planning smooth and obstacle-avoiding B-spline paths for autonomous mining vehicles. *IEEE T Autom Sci Eng* 2010; 7: 167–172.
17. Kieffer J, Cahill AJ and James MR. Robust and accurate time-optimal path-tracking control for robot manipulators. *IEEE T Robotic Autom* 1997; 13: 880–890.
18. Abdellatif H and Heimann B. Adapted time-optimal trajectory planning for parallel manipulators with full dynamic modeling. In: *Proceedings of the IEEE international conference on robotics and automation*, Barcelona, 18–22 April 2005, pp.411–416. New York: IEEE.
19. Bourbonnais F, Bigras P and Bonev IA. Minimum-time trajectory planning and control of a pick-and-place five-bar parallel robot. *IEEE/ASME T Mech* 2015; 20: 740–749.
20. Ur-Rehman R, Caro S, Chablat D, et al. Multi-objective path placement optimization of parallel kinematics machines based on energy consumption, shaking forces and maximum actuator torques: application to the Orthoglide. *Mech Mach Theory* 2010; 45: 1125–1141.
21. Huang MS, Hsu YL and Fung RF. Minimum-energy point-to-point trajectory planning for a motor-toggle servomechanism. *IEEE/ASME T Mech* 2012; 17: 337–344.
22. Chen CT and Liao TT. A hybrid strategy for the time- and energy-efficient trajectory planning of parallel platform manipulators. *Robot Cim: Int Manuf* 2011; 27: 72–81.
23. Piazzi A and Visioli A. Global minimum-jerk trajectory planning of robot manipulators. *IEEE T Ind Electron* 2000; 47: 140–149.
24. Macfarlane S and Croft EA. Jerk-bounded manipulator trajectory planning: design for real-time applications. *IEEE T Robotic Autom* 2003; 19: 42–52.
25. Gyorfi JS and Wu CH. A minimum-jerk speed-planning algorithm for coordinated planning and control of automated assembly manufacturing. *IEEE T Autom Sci Eng* 2006; 3: 454–462.
26. Gasparetto A, Lanzutti A, Vidoni R, et al. Validation of minimum time-jerk algorithms for trajectory planning of industrial robots. *J Mech Robot* 2011; 3: 031003.
27. Olabi A, Béarée R, Gibaru O, et al. Feedrate planning for machining with industrial six-axis robots. *Control Eng Pract* 2010; 18: 471–482.
28. Li HZ, Le MD, Gong ZM, et al. Motion profile design to reduce residual vibration of high-speed positioning stages. *IEEE/ASME T Mech* 2009; 14: 264–269.
29. Gasparetto A, Lanzutti A, Vidoni R, et al. Experimental validation and comparative analysis of optimal time-jerk algorithms for trajectory planning. *Robot Cim: Int Manuf* 2012; 28: 164–181.
30. Liu HS, Lai XB and Wu WX. Time-optimal and jerk-continuous trajectory planning for robot manipulators with kinematic constraints. *Robot Cim: Int Manuf* 2013; 29: 309–317.

31. Béarée R and Olabi A. Dissociated jerk-limited trajectory applied to time-varying vibration reduction. *Robot Cim: Int Manuf* 2013; 29: 444–453.
32. Guarino Lo and Bianco C. Minimum-jerk velocity planning for mobile robot applications. *IEEE T Robot* 2013; 29: 1317–1326.
33. Huang T, Wang PF, Mei JP, et al. Time minimum trajectory planning of a 2-DOF translational parallel robot for pick-and-place operations. *CIRP Ann: Manuf Techn* 2007; 56: 365–368.
34. Hu JF, Zhang XM and Zhan JQ. Trajectory planning of a novel 2-DOF high-speed planar parallel manipulator. In: Xiong C, Huang Y, Xiong Y, et al. (eds) *Intelligent robotics and applications*, vol. 5314. Berlin: Springer-Verlag, 2008, pp.199–207.
35. Lou YJ, Feng F and Wang MY. Trajectory planning and control of parallel manipulators. In: *Proceedings of the IEEE international conference on control and automation*, Christchurch, New Zealand, 9–11 December 2009, pp.1013–1018. New York: IEEE.
36. Tsai LW. Solving the inverse dynamics of a Stewart-Gough manipulator by the principle of virtual work. *J Mech Des: T ASME* 2000; 122: 3–9.
37. Chen CT and Liao TT. Trajectory planning of parallel kinematic manipulators for the maximum dynamic load-carrying capacity. *Meccanica* 2016; 51: 1653–1674.
38. Kucuk S. Maximal dexterous trajectory generation and cubic spline optimization for fully planar parallel manipulators. *Comput Electr Eng* 2016; 56: 634–647.
39. Kucuk S. Optimal trajectory generation algorithm for serial and parallel manipulators. *Robot Cim: Int Manuf* 2017; 48: 219–232.
40. Spong MW, Hutchinson S and Vidyasagar M. *Robot modeling and control*. New York: Wiley, 2006.
41. Zhang HJ, Su TT, Wu SH, et al. Simultaneous path planning and trajectory optimization for high-speed sorting system. *Int J Adv Robot Syst*. Epub ahead of print 27 September 2018. DOI: 10.1177/1729881418797870